Proceedings Paper:
Alanazi, N. and Susmel, L. orcid.org/0000-0001-7753-9176 (2020) The Theory of Critical Distances to predict static and dynamic strength of notched plain concrete under mixed-mode I/II loading. In: Iacoviello, F., Sedmak, A., Marsavina, L., Blackman, B., Ferro, G.A., Shlyannikov, V., Ståhle, P., Zhang, Z., Moreira, P.M.G.P., Božic, Ž. and Banks-Sills, L., (eds.) Procedia Structural Integrity. 1st Virtual European Conference on Fracture - VECF1, 29 Jun - 01 Jul 2020, Virtual conference. Elsevier , pp. 886-895.

https://doi.org/10.1016/j.prostr.2020.11.057

Available online at www.sciencedirect.com

ScienceDirect

Procedia Structural Integrity 28 (2020) 886–895

Structural Integrity Procedia

www.elsevier.com/locate/procedia

1st Virtual European Conference on Fracture

The Theory of Critical Distances to Predict Static and Dynamic Strength of Notched Plain Concrete under Mixed-Mode I/II Loading

N. Alanazi[a], L. Susmel[b]*

[a,b]*Department of Civil and Structural Engineering, The University of Sheffield, Mappin Street, Sheffield, S1 3JD, United Kingdom*

Abstract

The Theory of Critical Distances (TCD) is a powerful design tool capable of estimating the strength of notched/cracked materials by post-processing the linear-elastic stress fields ahead of the relevant stress raisers. The purpose of this paper is to reformulate the TCD to make it suitable for predicting the static/dynamic strength of notched unreinforced concrete subjected to Mixed-Mode I/II loading. The accuracy and reliability of the new extension of the TCD were checked using a large number of experimental results generated by testing plain concrete containing different geometrical features and tested under different loading rates and loading multiaxility. The predictions based on the proposed approach were seen to be within an error interval of ±30%. This level of accuracy is acceptable because it is within the scattering level of the experimental results used to calibrate the approach. These findings are promising and proving that this new reformulation of the TCD can be used to design notched plain concrete by modelling concrete as a linear-elastic, homogeneous, and isotropic material.

Keywords: The theory of Critical Distances; notched concrete; dynamic strength; static strength; Mixed-Mode I/II loading

1. Introduction

In real-life applications, concrete is subjected to different kinds of load, including dynamic loading (for instance, crashes, impact, or blast). Many studies show that concrete strength increases with the increase of the rate of applied loading (Malvar & Ross, 1998; Fu et al,. 1998; Biscoff & Perry, 1991; Williams, 1994). In more detail, the strength

* Corresponding author. Tel.: +44 (0) 114 222 5073; fax: +44 (0) 114 222 5700.
E-mail address: l.susmel@sheffield.ac.uk

2452-3216
10.1016/j.prostr.2020.11.057

of concrete under dynamic compression loading is seen to increase more than twice its static compression strength. Similarly, concrete's dynamic tensile strength is seen to increase more than six times its static tensile strength.

Nomenclature

a_f, b_f	material constants in the σ_f vs. $\dot{Z}$ relationship
a_k, b_k	material constants in the K_{Id} vs. $\dot{Z}$ relationship
a_L, b_L	material constants in the L vs. $\dot{Z}$ relationship
r_n	notch root radius
K_1	Mode I stress intensity factor
K_2	Mode II stress intensity factor
K_{Ic}	plane strain fracture toughness
K_{Id}	dynamic fracture toughness
$K_{t,b}$	stress concentration factor under pure bending
L	critical distance
$\dot{Z}$	reference dynamic variable
$\dot{\varepsilon}_p$	rate of the maximum opening normal strain
ρ	ratio between the Mode II and the Mode I stress intensity factor
σ_0	inherent strength
σ_{eff}	effective stress
σ_f	dynamic failure stress
$\sigma_n(r)$	normal linear-elastic stress perpendicular to the focus path
σ_{nom}	nominal stress
σ_p	failure value of the maximum opening normal stress
σ_y	normal stress parallel to y-axis
σ_{UTS}	ultimate tensile strength
θ, r	polar coordinates
θ_a	angle of orientation defining the focus path
θ_c	angle of orientation of the actual crack initiation plane
$\dot{\Delta}_c$	displacement rate parallel to the focus path

In the near future, additive manufacturing of concrete will be incorporated in the industry (Buswell et al., 2018). This technology will allow concrete components to have complex shapes. As a result, the stress gradients near these geometrical features will control the overall all strength of the concrete structure because they can trigger cracks leading to failure or shortening the designed life of the structure. To this end, the presence of stress concentration phenomena in concrete has not been investigated well (Pelekis & Susmel, 2017). Accordingly, this study proposes a new reformulation of the TCD to enable it to predict both static and dynamic strength of notched unreinforced concrete subjected to Mixed-Mode I/II loading.

2. TCD assessment of notched Brittle Materials Under Mode I Loading

According to the TCD (Taylor, 2007; Taylor, 2008), under Mode I quasi-static loading, a material containing a stress raiser will sustain the applied loading if the following condition is assured:

$$\sigma_{eff} \le \sigma_0 \tag{1}$$

In the above inequality, σ_0 is the inherent material strength, which is strictly equal to the ultimate tensile strength, σ_{UTS}, solely for those materials that are classified as brittle or quasi-brittle (Susmel & Taylor, 2008a; Taylor et al., 2004; Taylor, 2004). σ_{eff} is the effective stress that is calculated by post-processing the linear-elastic stress fields in the vicinity of the stress raiser being assessed

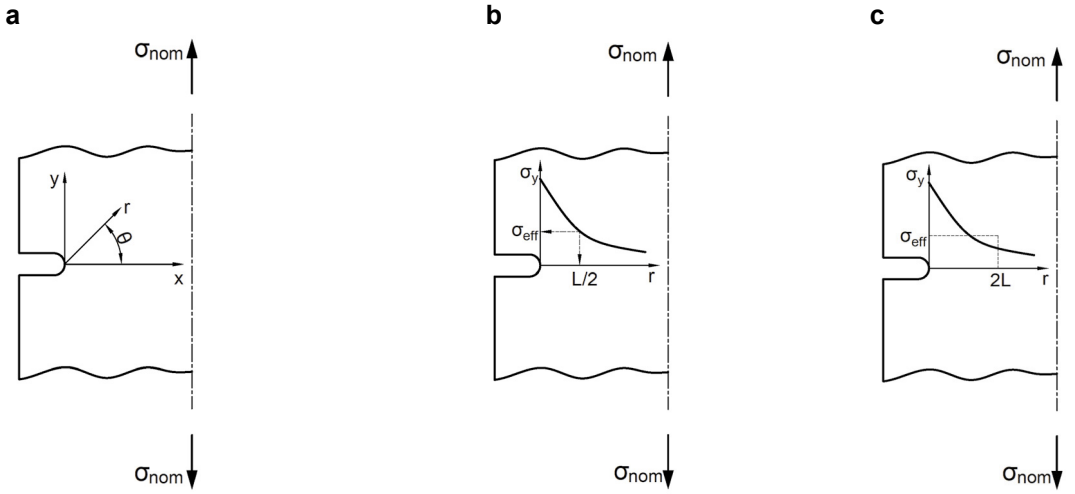

Fig.1 adopted coordinate system (a), calculation of σ_{eff} according to the Point Method (b), and the Line Method (c).

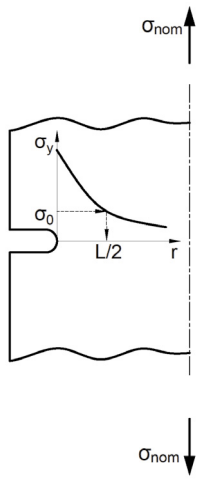

Fig. 2 Experimental determination of L using notched specimens according to the Poin Method.

According to the TCD, σ_{eff} can be determined in many different ways, including the Point Method (PM) and the Line Method (LM) as follows (Taylor, 2008; Susmel & Taylor, 2008a):

$$\sigma_{eff} = \sigma_y\left(\theta = 0, r = \frac{L}{2}\right) \quad \text{Point Method} \tag{2}$$

$$\sigma_{eff} = \frac{1}{2L}\int_0^{2L} \sigma_y\left(\theta = 0, r\right) dr \quad \text{Line Method} \tag{3}$$

The adopted local coordinate system and symbols to calculate the effective stress according to Eqs. (2) and (3) are schematically explained in Figures 1a to 1c, where σ_y is the linear-elastic stress perpendicular to the notch bisector. L is the so-called material critical distance. If the material plane strain fracture toughness, K_{Ic}, and inherent strength, σ_0, are known, the material critical distance can be directly calculated as follows (Taylor et al., 2004; Taylor, 2004; Jadallah et al., 2016):

$$L = \frac{1}{\pi}\left(\frac{K_{Ic}}{\sigma_0}\right)^2 \tag{4}$$

Since unreinforced concrete is modelled as being predominantly brittle under quasi-static loading (Neville & Brooks, 1987), its inherent strength is recommended to be taken equal to σ_{UTS} (Pelekis & Susmel, 2017). For brittle materials, that is when K_{Ic} is unknown, an alternative strategy can be followed to determine L (Susmel & Taylor 2010). In particular, according to Figure 2, initially, the linear-elastic stress field in the vicinity of a known notch is plotted in the incipient failure condition. From this stress-distance curve, the distance at which the local linear-elastic stress equals σ_{UTS} returns the value of L/2.

3. Extending the TCD to predict static/dynamic notched concrete strength under Mixed-Mode Loading

As discussed in the previous section, the TCD takes the material inherent strength equal to its ultimate tensile strength for brittle materials. Generally, testing material under bending shows higher flexural strength than its σ_{UTS}. However, previous investigations (Taylor, 200; Susmel & Taylor, 2008b) showed that the TCD calibrated by using σ_{UTS} is successful also in accommodating the increase in the strength due to bending. As far as concrete is concerned, bending is one of the commonly used material properties used in the design process. Therefore, in this study, the inherent strength is taken equal to the static/dynamic flexural strength of unnotched specimens.

Focusing attention on the dynamic strength, σ_f, Malvar and Crawford (1998) carried out a systematic study to investigate the variation of the dynamic tensile strength of concrete as a function of the local strain rate. They found that the dynamic tensile strength increases as the local strain rate increases. The tensile dynamic strength as a function of the local strain rate can be modelled by using simple power laws (Pelekis & Susme, 2017), with an evident change in the trend of the data as the local strain rate exceeds 1 mm/mm·s^{-1} (Malvar & Crawford, 1998). Similar studies were conducted on the dynamic fracture toughness of concrete, K_{Id}. The same monotonic response as the tensile dynamic strength was observed with an evident change as the local strain rate exceeds 1 mm/mm·s^{-1} (John & Shah, 1990; Lambert & Ross, 2000).

If $\dot{Z}$ is used to denote either the loading rate, the displacement rate, the stress rate, the strain rate, or the stress intensity factor rate, the increase in both the inherent strength and fracture toughness as the loading rate increases can be modelled, as a function of $\dot{Z}$, using the following power laws (Pelekis & Susmel, 2017; Yin et al., 2015):

$$\sigma_0\left(\dot{Z}\right) = a_f \dot{Z}^{b_f} \tag{5}$$

$$K_{Id}\left(\dot{Z}\right) = a_k \dot{Z}^{b_k} \tag{6}$$

where a_f, b_f, a_k, b_k are material constants either to be determined experimentally or to be derived theoretically.

After defining suitable expressions for describing the dynamic effect on both the inherent strength and the fracture toughness, definition (4) for the critical distance can directly be rewritten to include the material dynamic response as (Pelekis & Susmel, 2017; Yin et al., 2015):

$$L\left(\dot{Z}\right) = \frac{1}{\pi}\left[\frac{K_{Id}\left(\dot{Z}\right)}{\sigma_0\left(\dot{Z}\right)}\right]^2 = a_L \dot{Z}^{b_L} \tag{7}$$

where a_L and b_L are constants to be derived as soon as the constants in Eqs (5) and (6) are known.

Having presented definitions of the inherent strength and the critical distance to cover also the dynamic loading case, the subsequent step in the reasoning is establishing a rule suitable for locating the orientation of the focus path independently of the degree of multiaxiality of the applied loading. In this context, it is worth remembering that crack initiation and initial propagation in unreinforced concrete are due to Mode I opening stresses (Anderson, 2017; Karihaloo, 1995). Therefore, it is assumed that failure happens due to the initiation and initial propagation of cracks that are perpendicular to the maximum opening normal stress (Susmel & Taylor, 2008a). According to this assumption, the focus path is supposed to be a straight line emanating from the assumed crack initiation point and perpendicular to the maximum opening normal stress at the hot-spot itself (which is tangent to the surface at the crack initiation location and therefore coincides with the maximum principal stress). In this specific context, the focus path should coincide with the actual crack initiation plane.

To better clarify this aspect, consider Fig. 3a which shows a notched unreinforced concrete component subjected to a complex external system of forces that result in a local Mixed-Mode I/II stress state around the notch surface. In this case, the maximum opening stress is no longer at the notch tip. Instead, it could be found by solving Finite Element (FE) models or by using a proper analytical solution. Once the maximum normal opening stress is located, the focus path is simply a straight line emanating from the hot-spot and perpendicular to the surface itself at the origin. Further, as presented in Fig. 3a, the focus path takes an angle of θ_c from the notch bisector. This simple rule also works for those cases involving pure Mode I loading where the focus path coincides with the notch bisector (θ_c=0) because it is where the maximum opening normal stress operates, as in Fig. 3b. This indicates that this simple rule is in agreement with the classic Mode I TCD (Taylor 2007).

The dynamic variables used in this study and representing $\dot{Z}$ in Eqs (5) and (6) are the displacement rate, $\dot{\Delta}_c$, and the local maximum opening normal strain rate, $\dot{\varepsilon}_p$. $\dot{\Delta}_c$ is the displacement rate always taken parallel to the focus path, see Fig. 3. The displacement rate is used to check the consistency when $\dot{Z}$ is defined by using a global/nominal quantity. In contrast, $\dot{\varepsilon}_p$ is used to assess the accuracy of the approach being proposed when $\dot{Z}$ is defined via a local quantity.

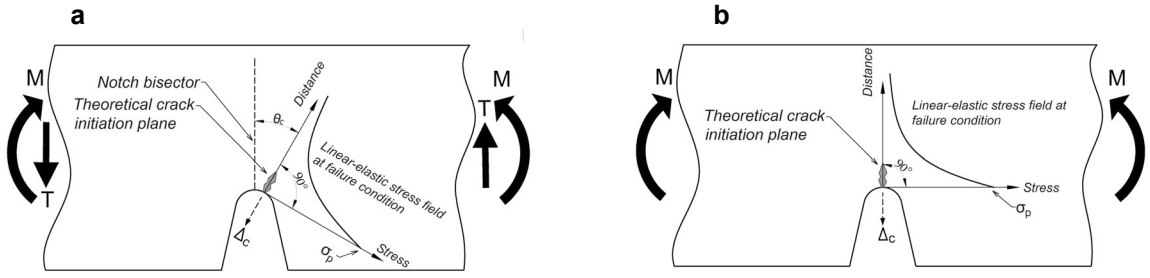

Fig. 3 Proposed orientation of the focus path for brittle materials under Mixed-Mode (I/II) loading (a) and under pure Mode (I) loading (b).

Having introduced suitable definitions for $\dot{Z}$, the TCD should be reformulated for making it suitable for assessing the strength of notched unreinforced concrete under Mixed-Mode static/dynamic loading. This starts with extending condition (1) by assuming that final breakage takes place when $\sigma_{\text{eff}}(\dot{Z})$ is equal to $\sigma_0(\dot{Z})$, with the latter being defined according to Eq. (5):

$$\sigma_{eff}\left(\dot{Z}\right)=\sigma_0\left(\dot{Z}\right)\Leftrightarrow \text{failure} \tag{8}$$

where $\sigma_{\text{eff}}(\dot{Z})$ can be calculated by modifying both definitions (2) and (3) as:

$$\sigma_{eff}\left(\dot{Z}\right)=\sigma_n\left(r=\frac{L\left(\dot{Z}\right)}{2}\right) \qquad \text{Point Method} \tag{9}$$

$$\sigma_{eff}\left(\dot{Z}\right)=\frac{1}{2L\left(\dot{Z}\right)}\int_{0}^{2L\left(\dot{Z}\right)}\sigma_{n}\left(r\right)dr \qquad \text{Line Method} \tag{10}$$

where $\sigma_n(r)$ is the normal linear-elastic stress perpendicular to the focus path (see Figure 3), r is the rectilinear coordinate parallel to the focus path, and $L(\dot{Z})$ is determined according to Eq. (7).

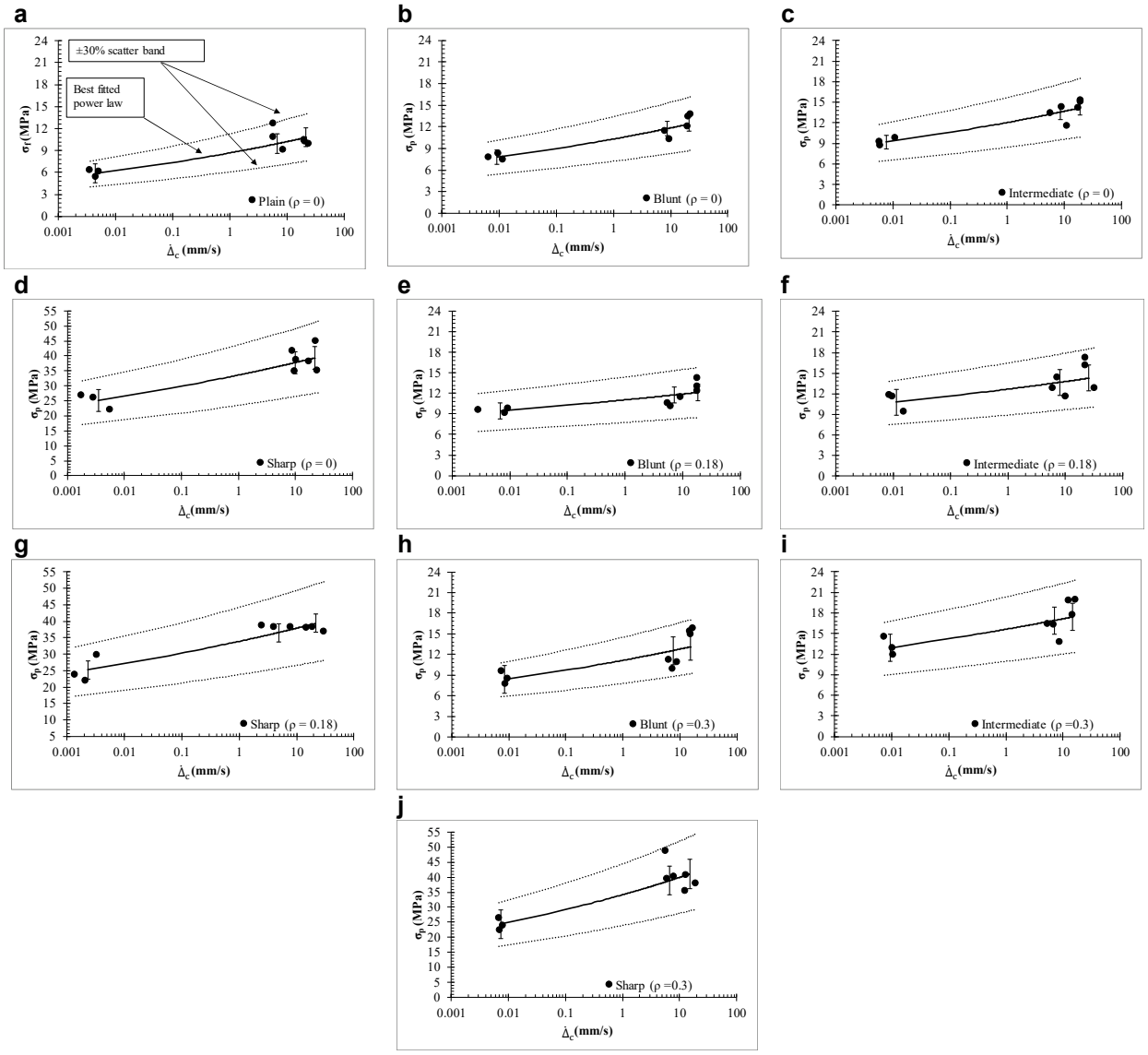

Fig. 4 Generated results of the un-notched (a) and notched specimens (b-j).

4. Experimental details and results

The accuracy of the new extension of the TCD being proposed was checked by generating a large number of experimental results. In more detail, symmetric and asymmetric bending tests were carried on beams having 100 mm X 100 mm square section and 500 mm long. Both unnotched and notched specimens had 50 mm net nominal depth.

Three notches of different sharpness were considered: the blunt notches had root radius, r_n, equal to 24 mm with a resulting stress concentration factor under bending, $K_{t,b}$, equal to 1.44, the intermediate notches had r_n = 12.5 mm ($K_{t,b}$ = 1.76), and, finally, sharp notches with r_n = 1.3 mm ($K_{t,b}$ = 4.51).

The specimens were manufactured according to the standardized procedure reported in Teychenné et al., (1975). 30 N/mm^2 Portland cement was mixed with river aggregate of 10 mm nominal size and fine aggregate of grade-M sand. The water-to-cement ratio was kept equal to 0.44 for all specimens. After casting, the specimens were removed from the moulds and directly stored in a controlled moist room until the time of testing.

Turning to the mechanical testing, three different loading multiaxiality were investigated. The level of loading multiaxiality was quantified by calculating index ρ, which is the ratio of the Mode II stress intensity factor, K_2, over the Mode I stress intensity factor, K_1. ρ was calculated analytically (Tada, 1985; Murakami, 1987) by replacing the notches with ideal zero tip cracks. Three different test configurations were considered in this study. First, standard three-point bending (3PB) set-up on symmetric notched specimens to produce Pure Mode I failure (ρ = 0). Asymmetric specimens tests under 3PB to generated Mixed-Mode I/II failures under ρ=0.18. Finally, Mixed-Mode I/II failure (ρ=0.3) was obtained by testing symmetric specimens under asymmetric four-point bending (4PB).

All of the tests were performed using a hydraulic actuator that was displacement-controlled with nominal travel speed ranging approximately between 0.002 mm/s to 35 mm/s. A high-speed/high-resolution camera was also synchronized with the loading cell to monitor the crack initiation process with the recorded peak force in the loading cell as well as to measure the local displacements around the tested notches. This was done by utilizing the Digital Image Correlation (DIC) technique. For every test, the high speed/high resolution videos confirm that the recorded peak force corresponded to a visible crack on the surface. This eliminates the possibility of having delays in the loading cell signal as well as confirms that the inertia of the loading piston did not influence the experimental values of the failure forces.

The stress distribution in the vicinity of stress raisers was determined numerically by solving FE models. The material in the specimens was treated as being linear-elastic, homogeneous, and isotropic. The notched samples were modelled using 4-node structural plane elements (plane 182) with gradual mesh refinement until convergence was reached in the vicinity of notches themselves.

Fig. 4 shows the experimental results as a function of $\dot{\Delta}_c$, which is calculated from the displacement given from the DIC and parallel to the focus path, see Fig. 3. Fig. 4a shows the dynamic failure strength of the un-notched specimens tested under pure Mode I 3PB. σ_f is determined according to the beam theory at the failure condition (i.e. the maximum recorded force). Further, this figure states that the data points fall within an intrinsic error interval of ±30% (Montgomery et al., 2012). Further, the same figure shows a good agreement between the data points and the fitted power law, as stated by (Malvar & Crawford, 1998). Figs 4b to 4j show the experimental results of the notched specimens under pure Mode I and Mixed-Mode loadings in terms of σ_p. σ_p is the maximum opening normal stress perpendicular to the focus path (see Fig. 3). Again, the same level of scattering in the notched specimens was observed where all the data points fall within a scatter band of ±30%.

The cracking behaviour of the notched specimens was observed visually. Independently of the loading rate and the Mode-Mixity level, the direct inspection of the cracked faces revealed that the cracks formed due to deboning between the aggregates and cement paste in those areas experiencing the maximum opening normal stresses - as explained in Section 3. After that, the initial crack propagation was seen to occur in the cement paste, which is immediately followed by unstable cracking until the final breakage of the specimens.

As explained in Section 3, the orientation of the focus path (θ_c) is assumed to coincide with the actual crack initiation plane, θ_a. In Fig. 5, both θ_c and θ_a are positive for specimens tested under 3PB (ρ = 0.18) and negative for specimens tested under 4PB (ρ = 0.3). The positive/negative signs are because the measurements were carried on opposite lateral surfaces. Fig 5 presents a comparison between the two angles. From the figure, it is possible to conclude that the proposed simple rule is capable of accurately capturing the actual orientation of the crack initiation plane independently of loading rate and Mode-Mixity level.

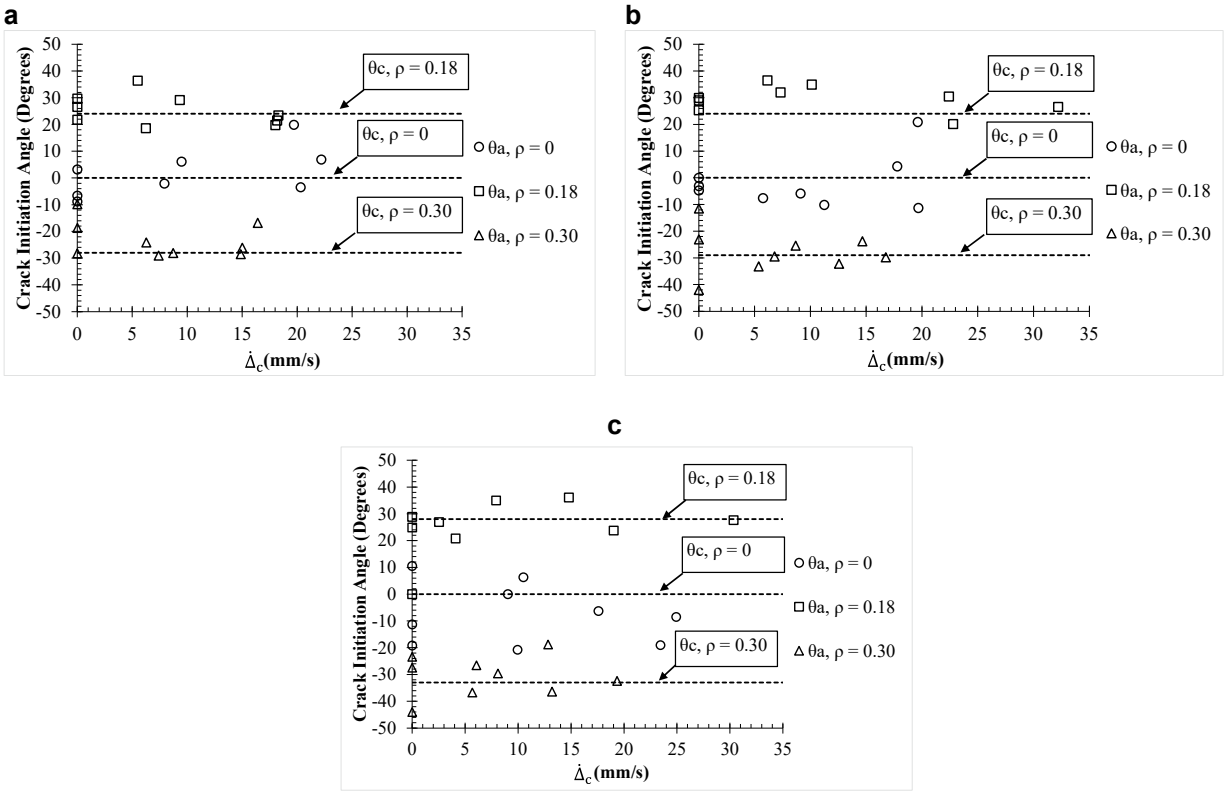

Fig. 5 Accuracy of the estimated orientation of the focus path compared to the actual orientation of the crack initiation plane of specimens containing blunt (a), intermediate (b), and sharp notches (c).

5. Verification of the new form of the PM and the LM

To check the accuracy of the new extension of the PM and LM in estimating the static/dynamic strength of notched plain concrete, the constants describing the dynamic strength in Eq (5) were calibrated by taking $\dot{Z}$ equal to $\dot{\Delta}_c$and $\dot{\varepsilon}_p$, as discussed in Section 3. By post-processing the results from the un-notched concrete specimens tested under Mode I static/dynamic loading (i.e. Fig. 4a) and applying the standard least-square method, the following values for a_f and b_f were derived:

$$\sigma_0\left(\dot{\Delta}_c\right) = 8.67\dot{\Delta}_c^{\,0.071} \tag{11}$$

$$\sigma_0\left(\dot{\varepsilon}_c\right) = 14.58\dot{\varepsilon}_c^{\,0.078} \tag{12}$$

The determination of a_L and b_L in Eq (7) to describe the relationship between L and $\dot{Z}$ was done by following the methodology explained in Fig. 2. This was performed by post-processing the Mode I results from the un-notched specimens and the sharply notched samples (Fig. 4a and 4j), obtaining:

$$L\left(\dot{\Delta}_c\right) = 4.7\dot{\Delta}_c^{\,-0.03} \tag{13}$$

$$L\left(\dot{\varepsilon}_c\right) = 3.3\dot{\varepsilon}_c^{\,-0.03} \tag{14}$$

Having presented the calibration equations for the inherent strength and the critical distance, σ_{eff} was then calculated according to the PM and LM using to Eqs (9) and (10). This was done by post-processing the linear- elastic stress fields at failure condition in the vicinity of notches for all notched specimens being considered. The accuracy of the estimations of both the PM and LM were quantified by calculating the error as follows:

$$\text{Error} = \frac{\sigma_{\text{eff}}\left(\dot{Z}\right) - \sigma_0\left(\dot{Z}\right)}{\sigma_0\left(\dot{Z}\right)} \times 100 \tag{15}$$

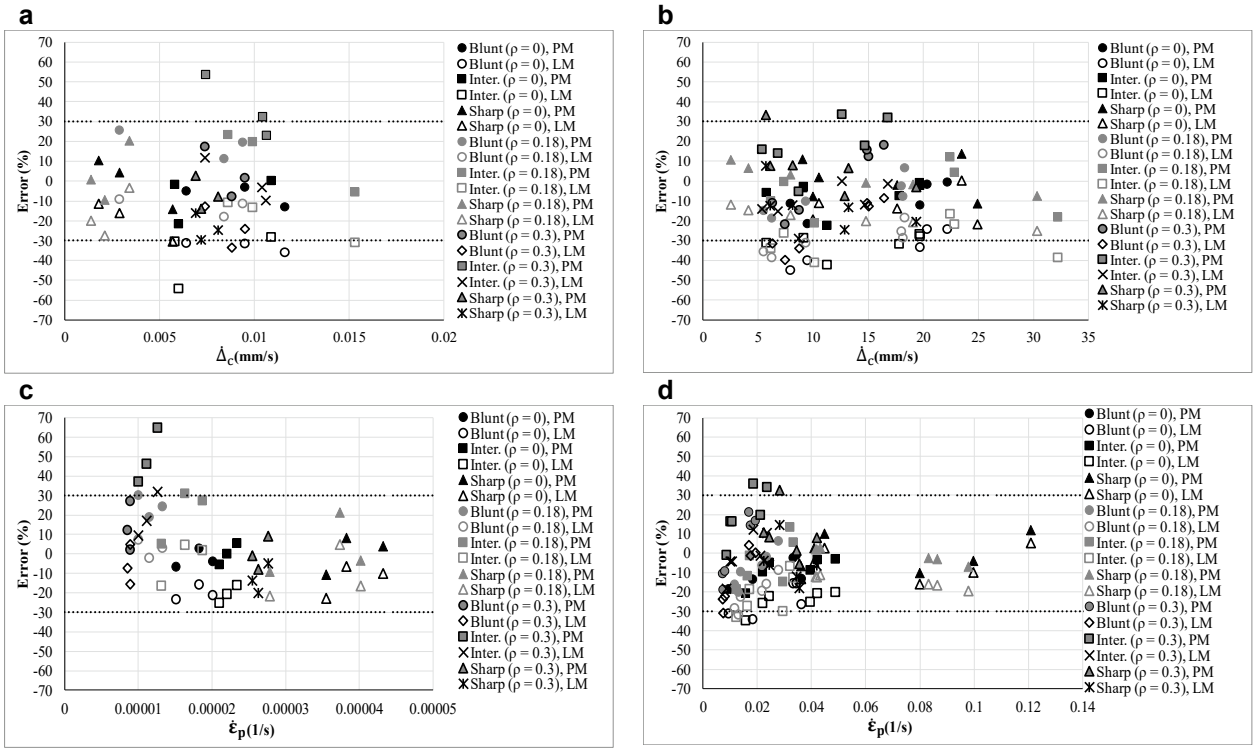

Fig. 6. Accuracy of the proposed extension of the TCD in assessing the static/dynamic strength as a function of local displacement rate (a,b) and maximum opening strain rate (c,d).

Fig. 6 summarizes the overall accuracy of the new proposed approach. In more details, Figs 6a and 6c show the predictions made under quasi-static loading, whereas Figs 6b and 6d those obtained under dynamic loading.

Fig. 6 makes it evident that the predictions due to the PM and LM fall within an error internal of ±30%, which is seen to be within the intrinsic scattering level characterising the experimental results. These predictions are considered accurate as it is impossible to derive more accurate results than the scattering level of the data used to calibrate the approach. Further, as expected, calibrating the TCD with local quantity (i.e. $\dot{\varepsilon}_p$) in the vicinity of the estimated crack initiation points resulted in more accurate estimates.

6. Conclusion

- The strength of concrete weakened by notches increases with the increase of the loading rate.
- Opening normal stresses govern the cracking behaviour, with this holding true independently of loading rate and level of loading multiaxiality.
- The suggestions to define the orientation of the focus path are seen to be accurate in estimating the orientation of the crack initiation plane.

- Taking advantage of the TCD features, un-reinforced concrete can be designed by modelling concrete as a linear-elastic, homogeneous, and isotropic material.
- The new formulation of the TCD confirms that the strength of unreinforced notched concrete can be estimated within ±30% which is found to be accurate because the predictions are as scattered as the data points used to calibrate the approach itself.

References

Anderson, T.L., 2017. Fracture mechanics: fundamentals and applications. CRC press.

Bischoff, P.H. and Perry, S.H., 1991. Compressive behaviour of concrete at high strain rates. Materials and structures, 24(6), pp.425-450.

Buswell, R.A., de Silva, W.L., Jones, S.Z. and Dirrenberger, J., 2018. 3D printing using concrete extrusion: A roadmap for research. Cement and Concrete Research, 112, pp.37-49.

Fu, H.C., Erki, M.A. and Seckin, M., 1991. Review of effects of loading rate on concrete in compression. Journal of structural engineering, 117(12), pp.3645-3659.

Jadallah, O., Bagni, C., Askes, H. and Susmel, L., 2016. Microstructural length scale parameters to model the high-cycle fatigue behaviour of notched plain concrete. International Journal of Fatigue, 82, pp.708-720.

John, R. and Shah, S.P., 1990. Mixed-mode fracture of concrete subjected to impact loading. Journal of Structural Engineering, 116(3), pp.585-602.

Karihaloo, B.L., 1995. Fracture mechanics & structural concrete. Longman Scientific and Technical.

Lambert, D.E. and Ross, C.A., 2000. Strain rate effects on dynamic fracture and strength. International Journal of Impact Engineering, 24(10), pp.985-998.

Malvar, L.J. and Crawford, J.E., 1998, August. Dynamic increase factors for steel reinforcing bars [C]. In 28th DDESB Seminar. Orlando, USA.

Malvar, L.J. and Ross, C.A., 1998. Review of static and dynamic properties of concrete in tension. ACI Materials Journal, 95(6), pp.735-739.

Montgomery, D.C., Peck, E.A. and Vining, G.G., 2012. Introduction to linear regression analysis (Vol. 821). John Wiley & Sons.

Murakami, Y., 1987. Handbook of stress intensity factors. In Pergamon Press, Oxford (UK). (p. 1011).

Neville, A.M. and Brooks, J.J., 1987. Concrete technology (pp. 242-246). England: Longman Scientific & Technical.

Pelekis, I. and Susmel, L., 2017. The Theory of Critical Distances to assess failure strength of notched plain concrete under static and dynamic loading. Engineering Failure Analysis, 82, pp.378-389.

Susmel, L. and Taylor, D., 2008a. The theory of critical distances to predict static strength of notched brittle components subjected to mixed-mode loading. Engineering Fracture Mechanics, 75(3-4), pp.534-550.

Susmel, L. and Taylor, D., 2008b. On the use of the Theory of Critical Distances to predict static failures in ductile metallic materials containing different geometrical features. Engineering Fracture Mechanics, 75(15), pp.4410-4421.

Susmel, L. and Taylor, D., 2010. The Theory of Critical Distances as an alternative experimental strategy for the determination of KIc and ΔKth. Engineering Fracture Mechanics, 77(9), pp.1492-1501.

Tada, H., 1985. The stress analysis of cracks handbook, Paris Productions. Inc., St. Louis.

Taylor, D., 2004. Predicting the fracture strength of ceramic materials using the theory of critical distances. Engineering Fracture Mechanics, 71(16-17), pp.2407-2416.

Taylor, D., 2007. The Theory of Critical Distances: A new perspective in fracture mechanics. Elsevier, Oxford, UK.

Taylor, D., 2008. The theory of critical distances. Engineering Fracture Mechanics, 75(7), pp.1696-1705.

Taylor, D., Merlo, M., Pegley, R. and Cavatorta, M.P., 2004. The effect of stress concentrations on the fracture strength of polymethylmethacrylate. Materials Science and Engineering: A, 382(1-2), pp.288-294.

Teychenné, D.C., Franklin, R.E., Erntroy, H.C. and Marsh, B.K., 1975. Design of normal concrete mixes. HM Stationery Office.

Williams, M.S., 1994. Modeling of local impact effects on plain and reinforced concrete. Structural Journal, 91(2), pp.178-187.

Yin, T., Tyas, A., Plekhov, O., Terekhina, A. and Susmel, L., 2015. A novel reformulation of the Theory of Critical Distances to design notched metals against dynamic loading. Materials & Design, 69, pp.197-212.